



## Study of Density Distributions, Elastic Electron Scattering form factors and reaction cross sections of ${}^9\text{C}$ , ${}^{12}\text{N}$ and ${}^{23}\text{Al}$ exotic nuclei

Adel K. Hamoudi, Gaith N. Flaiyh , Ahmed N. Abdullah\*

Department of Physics, College of Science, University of Baghdad, Baghdad, Iraq.

### Abstract

The ground state densities of unstable proton-rich  ${}^9\text{C}$ ,  ${}^{12}\text{N}$  and  ${}^{23}\text{Al}$  exotic nuclei are studied via the framework of the two-frequency shell model (TFSM) and the binary cluster model (BCM). In TFSM, the single particle harmonic oscillator wave functions are used with two different oscillator size parameters  $\beta_c$  and  $\beta_v$ , where the former is for the core (inner) orbits and the latter is for the valence (halo) orbits. In BCM, the internal densities of the clusters are described by single particle Gaussian wave functions. The long tail performance is clearly noticed in the calculated proton and matter density distributions of these nuclei. The structure of the valence proton in  ${}^9\text{C}$  and  ${}^{12}\text{N}$  is a pure ( $1p_{1/2}$ ) configuration while that for  ${}^{23}\text{Al}$  is mixed configurations with dominant ( $2s_{1/2}$ ). Elastic electron scattering proton form factors for  ${}^9\text{C}$ ,  ${}^{12}\text{N}$  and  ${}^{23}\text{Al}$  are studied using the plane wave born approximation (PWBA). It is found that the major difference between the calculated form factors of unstable (exotic) [ ${}^9\text{C}$ ,  ${}^{12}\text{N}$ ,  ${}^{23}\text{Al}$ ] nuclei and those of stable [ ${}^{12}\text{C}$ ,  ${}^{14}\text{N}$ ,  ${}^{27}\text{Al}$ ] nuclei is attributed firstly to the influence of the proton density distributions of the last proton in unstable nuclei and secondly to the difference in the center of mass correction which depends on the mass number and the size parameter  $\beta$  (which is assumed in this case equal to the average of  $\beta_c$  and  $\beta_v$ ). The reaction cross sections for  ${}^9\text{C}$ ,  ${}^{12}\text{N}$  and  ${}^{23}\text{Al}$  are studied by means of the Glauber model with an optical limit approximation using the ground state densities of the projectile and target, where these densities are described by single Gaussian functions. The calculated reaction cross sections of  ${}^9\text{C}$ ,  ${}^{12}\text{N}$  and  ${}^{23}\text{Al}$  at high energy are in good agreement with the data. The analysis of the present study supports the halo structure of these nuclei.

**Keywords:** proton-rich exotic nuclei; shell model calculations; elastic electron scattering form factor; density distributions; root mean square radii of halo nuclei

## دراسة توزيعات الكثافة، عوامل التشكل للاستطارة الالكترونية المرنة و المقاطع العرضية للتفاعل للنوى الغريبة ${}^{23}\text{Al}$ و ${}^{12}\text{N}$ , ${}^9\text{C}$

عادل خلف حمودي، غيث نعمة فليح ، أحمد نجم عبدالله\*

قسم الفيزياء ، كلية العلوم، جامعة بغداد، بغداد، العراق

### الخلاصة

تم حساب توزيعات الكثافة للنوى الغريبة غير المستقرة والغنية بالبروتونات  ${}^9\text{C}$ ,  ${}^{12}\text{N}$  و  ${}^{23}\text{Al}$  باستخدام نموذج القشرة ذو الترددات (TFSM) والأنموذج العنقودي الثنائي (BCM). في أنموذج القشرة ذو الترددات استخدمت الدوال الموجية للجسيمة المفردة لجهد المتذبذب التوافقي مع قيمتين مختلفتين للتأثير التوافقي احدهما  $(\beta_c)$  للقلب و الاخرى  $(\beta_v)$  للنوكليونات الفعالة (الموجودة خارج القلب النووي). في الأنموذج العنقودي

\*Email: Ahmednajim1979@yahoo.com

الثنائي تم وصف الكثافة الداخلية للعنقودين باستخدام دالة غاوس للجسيمة المفردة. الامتداد الطويل ظهر بوضوح في توزيعات الكثافة البروتونية والكتلية لهذه النوى. اوضحت هذه الدراسة بان النيوكليون الفعال للنوى  $^9\text{C}$  و  $^{12}\text{N}$  له التشكيل النقي ( $1p_{1/2}$ ) اما النيوكليون الفعال للنواة  $^{23}\text{Al}$  فانه يتركب من حالات ممتزجة وبهيمنة التشكيل ( $2s_{1/2}$ ). لقد تم تحليل نتائج عوامل التشكل المرنة لبروتونات هذه النوى بواسطة تقريب بورن للموجة المستوية. وجد ان الاختلاف بين عوامل التشكل للنوى الغريبة [ $^{23}\text{Al}$ ,  $^{12}\text{N}$ ,  $^9\text{C}$ ] ونظيرتها المستقرة [ $^{27}\text{Al}$ ,  $^{14}\text{N}$ ,  $^{12}\text{C}$ ] يعود الى التباين في توزيعات الكثافة البروتونية لهذه النوى والنتائج بصورة رئيسية من وجود بروتون في مدارات الهالة وكذلك التباين في عامل تصحيح مركز الكتلة والذي يعتمد على العدد الكتلي وثابت المتذبذب التوافقي ( $\beta$ ). المقاطع العرضية للتفاعل لهذه النوى عند الطاقات العالية تم دراستها باستخدام نموذج كلوبر باستخدام توزيع الكثافة للحالة الارضية للنواة القذيفة والهدف، حيث ان هذه الكثافات توصف بواسطة دوال غاوس للجسيمة المنفردة. ان حسابات المقاطع العرضية للتفاعل لهذه النوى تتفق بشكل جيد مع القيم العملية.

## Introduction

Since the discoveries of neutron halo in exotic light neutron-rich nuclei in the mid-eighties [1,2], studies on halo phenomena have become a hot point in nuclear physics. The neutron halo is a weakly bound exotic nuclear state where the valence neutrons are spatially decoupled from a tightly bound core and the wave function extends into the classically forbidden region [3]. The cause of halo phenomena lies in both the small separation energy of the last few nucleons and their occupation on the orbits with low angular momentum ( $l = 0, 1$ ) [4], which allow the wave function of the valence nucleons to extend to large radii [5]. The observation of large total interaction cross sections for  $^{11}\text{Li}$ ,  $^{11}\text{Be}$ , and  $^{14}\text{Be}$  by Tanihata *et al.* [1] showed that halo is probably present in many neutron-rich nuclei close to the drip line and initialized intensive experimental and theoretical work on neutron-rich nuclei. Such a behavior shows up also on the proton-rich side of the chart of nuclei [5]. But the study of proton-rich nuclei is scarce as compared with that of neutron-rich nuclei. It is believed that it is slightly hard for proton-rich nuclei to form the halo structure because of Coulomb barrier [6], which hinder the proton to penetrate into the out region of the nuclear-core [7].

Electron-nucleus scattering has proven to be an excellent tool for the study of nuclear structure, especially for the research of electromagnetic properties of nuclei. It has provided much reliable information on charge density distributions of stable nuclei. Thus, we consider that the electron-nucleus scattering is a better way for the precise investigation of the extended charge distribution of the exotic proton-rich nuclei. Unfortunately, the electron scattering on exotic nuclei was not possible in the past because of the difficulty of making targets from unstable nuclei [8]. Recently a new collider of electron and unstable nucleus is under construction at RIKEN in Japan [9]. A similar collider at GSI in Germany [10] was also approved by the German government and will be built immediately. So the scattering of electron from unstable nuclei will be available soon. These new facilities will provide a good opportunity to study the charge density distributions of unstable nuclei by elastic electron scattering.

As it follows from the analyses of the interaction cross section [11],  $^{12}\text{N}$  nucleus exhibits significant halo structures. Warner *et al.* [12] measured the total reaction cross section ( $\sigma_R$ ) of  $^{12}\text{N}$  on a Si target at energy of about 30 A MeV. The result for  $\sigma_R$  was  $1840 \pm 55 \text{mb}$ .

Ozawa *et al.* [13] studied the interaction cross section for  $\sigma_7$   $^9\text{C}$  on a carbon target at 720 A MeV. The result for  $\sigma_7$  was  $834 \pm 18 \text{mb}$ . They also studied the root mean square (rms) matter radii of  $^9\text{C}$  using the Glauber-type calculation. Their result was  $2.42 \pm 0.03 \text{fm}$ . Hong *et al.* [14] used the asymptotic normalization coefficient to obtain the root mean square (rms) matter radii of  $^9\text{C}$ . The result for rms was  $2.62 \pm 0.55 \text{fm}$ .

The discovered proton halo nucleus of  $^{23}\text{Al}$  is investigated in the nonlinear relativistic mean-field (RMF) model [15]. The halo structure of  $^{23}\text{Al}$  has been confirmed by Fang *et al.* [16].

The total nuclear reaction cross section ( $\sigma_{tot}$ ) is one of the most important physical quantities characterizing the properties of nuclear reaction [17]. It is very useful for extracting fundamental information about the nuclear size and the density distributions of neutrons and protons in nucleus. In

particular, the neutron halo has been found by measuring the total reaction cross section induced by radioactive nuclear beams [1, 18]. The definition of the reaction cross section ( $\sigma_R$ ) and the interaction cross section ( $\sigma_I$ ) are [19]:  $\sigma_R = \sigma_{tot} - \sigma_{ela}$  and  $\sigma_I = \sigma_R - \sigma_{inela}$ , where  $\sigma_{ela}$  and  $\sigma_{inela}$  are the elastic and inelastic scattering cross sections, respectively. At high energy (above several hundred MeV/nucleon), it is known that  $\sigma_R$  is approximated by  $\sigma_I$  ( $\sigma_R \approx \sigma_I$ ) because the contribution of the inelastic scattering is low [20, 21].

One of the widely used models for analyzing the interaction and the reaction cross sections of nucleus-nucleus scattering is the Glauber model [22]. In ref. [23], a simple Glauber model was used to connect the density distributions and cross sections. Although this model is simple, it shows reasonable results of many cases for the reactions of the stable and exotic nuclei. A modified microscopic Glauber theory [22, 24] was used to investigate the reaction projectile-target collisions at low and intermediate energies. The calculated reaction cross sections [22, 24] at intermediate energies were in good agreement with the experimental data.

In the present study, we analyze the ground state densities, elastic electron scattering proton form factors and reaction cross sections of unstable proton-rich  ${}^9\text{C}$ ,  ${}^{12}\text{N}$  and  ${}^{23}\text{Al}$  exotic nuclei. The structure of the valence proton in  ${}^9\text{C}$  and  ${}^{12}\text{N}$  is a pure ( $1p_{1/2}$ ) configuration while that for  ${}^{23}\text{Al}$  is mixed configurations with dominant ( $2s_{1/2}$ ).

Elastic electron scattering proton form factors for these exotic halo nuclei are studied through combining the proton density distribution, obtained by the TFMS, with the PWBA. The difference between the calculated form factors of unstable (exotic) [ ${}^9\text{C}$ ,  ${}^{12}\text{N}$ ,  ${}^{23}\text{Al}$ ] nuclei and those of stable [ ${}^{12}\text{C}$ ,  ${}^{14}\text{N}$ ,  ${}^{27}\text{Al}$ ] nuclei is attributed firstly to the influence of the proton density distributions of the last proton in unstable nuclei and secondly to the difference in the center of mass correction which depends on the mass number and the size parameter  $\beta$  (which is assumed in this case equal to the average of  $\beta_c$  and  $\beta_v$ ). The reaction cross sections for  ${}^9\text{C}$  [ ${}^{12}\text{N}$ ,  ${}^{23}\text{Al}$ ] is examined by means of the Glauber model with an optical limit approximation using the ground state densities of the projectile and target. The calculated reaction cross sections at high energies are in good agreement with the data. The analysis of the present study suggests the halo structure of these exotic nuclei.

## Theory

The one-body operator of the longitudinal transition density for point protons (with isospin  $t_z = 1/2$ ) or neutrons ( $t_z = -1/2$ ) is given by [25]

$$\hat{\rho}_{\Delta J, t_z}^L = \sum_{k=1}^A e(t_z) \frac{\delta(r - r_k)}{r_k^2} Y_{\Delta J, M_{\Delta J}}(\Omega_{r_k}), \quad (1)$$

with

$$e(t_z) = \frac{1 + 2t_z(k)}{2}.$$

In Eq. (1), the superscript ( $L$ ) in the operator  $\hat{\rho}_{\Delta J, t_z}^L$  stands for a longitudinal operator,  $Y_{\Delta J, M_{\Delta J}}(\Omega_{r_k})$  and  $\delta(\vec{r} - \vec{r}_k)$  are the spherical harmonic and Dirac delta functions, respectively. The multipolarity  $\Delta J$  of the transition is restricted by the following angular momentum and parity selection rules:

$$|J_i - J_f| \leq \Delta J \leq J_i + J_f$$

and

$$\pi_i \pi_f = (-1)^{\Delta J} \quad (\text{for Coulomb transitions}).$$

The reduced matrix element of Eq. (1) is expressed as [25]

$$\langle J_f \| \hat{\rho}_{\Delta J, t_z}^L(\vec{r}) \| J_i \rangle = \frac{1}{\sqrt{4\pi(2J_i + 1)}} \sum_{ab} \text{OBDM}(J_f, J_i, \Delta J, a, b, t_z) \langle j_a \| Y_{\Delta J} \| j_b \rangle R_{n_a l_a}(r) R_{n_b l_b}(r), \quad (2)$$

where  $a$  and  $b$  label single-particle states for the considered shell model space, i.e.  $|a\rangle = |n_a l_a\rangle |j_a m_a\rangle$  and  $|b\rangle = |n_b l_b\rangle |j_b m_b\rangle$ , the states  $|J_i\rangle$  and  $|J_f\rangle$  are characterized by the model

space wave functions,  $R_{n_p l_p}(r)$  is the radial part of the harmonic oscillator wave function,  $\langle j_a || Y_{\Delta J} || j_b \rangle$  is the reduced matrix element of the spherical harmonic,  $OBDM(J_f, J_i, \Delta J, a, b, t_z)$  is the proton ( $t_z = 1/2$ ) or neutron ( $t_z = -1/2$ ) one body density matrix element given by the second quantization as [25]

$$OBDM(J_f, J_i, \Delta J, a, b, t_z) = \frac{\langle J_f || [a_{a, t_z}^+ \otimes \tilde{a}_{b, t_z}]^{\Delta J} || J_i \rangle}{\sqrt{2\Delta J + 1}}. \quad (3)$$

As the model space wave functions have good isospin, it is appropriate to evaluate the  $OBDM$  elements by means of isospin-reduced matrix elements. The relation between these triply reduced  $OBDM$  and the proton or neutron  $OBDM$  of Eq. (2) is given by [25]

$$OBDM(t_z) = (-1)^{T_f - T_z} \sqrt{2} \begin{pmatrix} T_f & 0 & T_i \\ -T_z & 0 & T_z \end{pmatrix} OBDM(\Delta T = 0) / 2 \\ + 2t_z (-1)^{T_f - T_z} \sqrt{6} \begin{pmatrix} T_f & 1 & T_i \\ -T_z & 0 & T_z \end{pmatrix} OBDM(\Delta T = 1) / 2 \quad (4)$$

where the triply reduced  $OBDM(\Delta T)$  elements are given in terms of the second quantization as

$$OBDM(i, f, \Delta J, \alpha, \beta, \Delta T) = \frac{\langle \Gamma_f || [a_{\alpha}^+ \otimes \tilde{a}_{\beta}]^{\Delta J, \Delta T} || \Gamma_i \rangle}{\sqrt{2\Delta J + 1} \sqrt{2\Delta T + 1}} \quad (5)$$

Here, Greek symbols are utilized to indicate quantum numbers in coordinate space and isospace (i.e.,  $\alpha \equiv at_a$ ,  $\beta \equiv bt_b$ ,  $\Gamma_i \equiv J_i T_i$  and  $\Gamma_f \equiv J_f T_f$ ).

The  $OBDM(\Delta T)$  elements contain all of the information about transitions of given multiplicities which are embedded in the model space wave functions. To obtain these  $OBDM$  elements, we perform shell model calculations by OXBASH code [26] using realistic effective interactions.

For the ground state density distribution, we have  $n_a = n_b$ ,  $l_a = l_b$ ,  $j_a = j_b$ ,  $J_i = J_f$  and  $\Delta J = 0$ , then Eq. (2) becomes as

$$\rho_{t_z}(r) \equiv \langle J_i || \hat{\rho}_{\Delta J=0, t_z}^L(\vec{r}) || J_i \rangle \\ = \frac{1}{\sqrt{4\pi(2J_i + 1)}} \sum_{ab} OBDM(J_i, J_i, 0, a, b, t_z) \langle j_a || Y_0 || j_b \rangle R_{n_a l_a}(r) R_{n_b l_b}(r), \quad (6)$$

where

$$\langle j_a || Y_0 || j_b \rangle = \left\langle j_a \left\| \frac{1}{\sqrt{4\pi}} \right\| j_b \right\rangle = \frac{1}{\sqrt{4\pi}} \langle j_a || 1 || j_b \rangle = \frac{1}{\sqrt{4\pi}} \sqrt{2j_a + 1} \delta_{j_a j_b}. \quad (7)$$

The average occupation number in each orbit  $n_{a, t_z}$  is given by

$$n_{a, t_z} = \sqrt{\frac{2J_a + 1}{2J_i + 1}} OBDM(J_i, J_i, 0, a, a, t_z). \quad (8)$$

As the exotic halo nuclei are oversized and easily broken systems consisting of a compact core plus a number of outer nucleons loosely bound and spatially extended far from the core, it is suitable to separate the ground state matter density distribution  $\rho_{t_z, m}(r)$  into two parts. The first part is connected to the core nucleons  $\rho_{t_z, c}(r)$  while the second is connected to the valence (halo) nucleons  $\rho_{t_z, v}(r)$ , (for simplicity, the subscript  $t_z$  in these densities will be dropped), i.e.

$$\rho_m(r) = \rho_c(r) + \rho_v(r). \quad (9)$$

Two approaches are utilized for calculating the ground state densities of exotic nuclei, these are the two frequency shell model (TFSM) and the binary cluster model (BCM).

In TFMS [27, 28], the harmonic oscillator wave functions (HO) are used with two different oscillator size parameters  $\beta_c$  (for core nucleons) and  $\beta_v$  (for halo nucleons). This approach permits to work freely on each part by changing  $\beta_{c(v)}$  till obtaining a fit with observed data. Furthermore, the matter density of Eq. (9) may also be expressed as

$$\rho_m(r) = \rho^p(r) + \rho^n(r), \quad (10)$$

where  $\rho^p(r)$  and  $\rho^n(r)$  are the ground state proton and neutron densities of halo nuclei expressed as

$$\rho^p(r) = \rho_c^p(r) + \rho_v^p(r) \quad (11)$$

and

$$\rho^n(r) = \rho_c^n(r) + \rho_v^n(r). \quad (12)$$

The normalization conditions for the ground state densities given in Eqs. (9-12) are

$$g = 4\pi \int_0^\infty \rho_g(r) r^2 dr, \quad (13)$$

and the corresponding rms radii are

$$\langle r^2 \rangle_g^{1/2} = \frac{4\pi}{g} \int_0^\infty \rho_g(r) r^4 dr, \quad (14)$$

where  $\rho_g(r)$  corresponds to the one of the densities [ $\rho_m(r)$ ,  $\rho_c(r)$ ,  $\rho_v(r)$ ,  $\rho^p(r)$ ,  $\rho^n(r)$ ] and  $g$  corresponds to the number of nucleon in each case.

Next we use the plane wave born approximation (PWBA) to study the elastic electron scattering form factors from considered nuclei. In the PWBA, the incident and scattered electron waves are represented by plane waves. The elastic proton form factor is simply given by the Fourier-Bessel transform of the ground state proton density distribution obtained by TFMS, i.e.

$$F(q) = \frac{4\pi}{Z} \int_0^\infty \rho^p(r) j_0(qr) r^2 dr, \quad (15)$$

where  $j_0(qr)$  is the spherical Bessel function of order zero and  $q$  is the momentum transfer from the incident electron to the target nucleus. Inclusion the corrections of the finite nucleon size  $F_{fs}(q) = \exp(-0.43q^2/4)$  and the center of mass  $F_{cm}(q) = \exp(b^2q^2/4A)$  in the calculations needs multiplying the form factor of Eq. (15) by these corrections.

In BCM [29], the exotic nuclei are considered as composite projectiles of mass  $A_p$  and described, in figure 1, as core and valence clusters, of masses  $A_c$  and  $A_v$  bounded with a state of relative motion. It is assumed that  $A_c \geq A_v$ . For simplicity, the internal densities of clusters are described by single Gaussian functions with ranges  $\alpha_c$  and  $\alpha_v$ ,

$$\rho_c(r) = A_c g^{(3)}(\alpha_c, r), \quad (16)$$

$$\rho_v(r) = A_v g^{(3)}(\alpha_v, r),$$

where  $g^{(3)}$  is the normalized 3-dimensional Gaussian function

$$g^{(3)}(\alpha_{c(v)}, r) = \frac{1}{\pi^{3/2} \alpha_{c(v)}^3} \exp(-r^2 / \alpha_{c(v)}^2), \quad \int g^{(3)}(\alpha_{c(v)}, r) d\vec{r} = 1, \quad \langle r^2 \rangle_{c(v)} = 3\alpha_{c(v)}^2 / 2. \quad (17)$$

Upon convoluting the intrinsic cluster densities with their center of mass (c.m.) motions about the c.m. of the projectile, the composite projectile density is given by [29]

$$\rho_p(r) = A_c g^{(3)}(\hat{\alpha}_c, r) + A_v g^{(3)}(\hat{\alpha}_v, r) \quad (18)$$

with range parameters

$$\hat{\alpha}_v^2 = \alpha_v^2 + \left( \frac{A_c \alpha}{A_v + A_c} \right)^2, \quad \hat{\alpha}_c^2 = \alpha_c^2 + \left( \frac{A_v \alpha}{A_v + A_c} \right)^2. \quad (19)$$

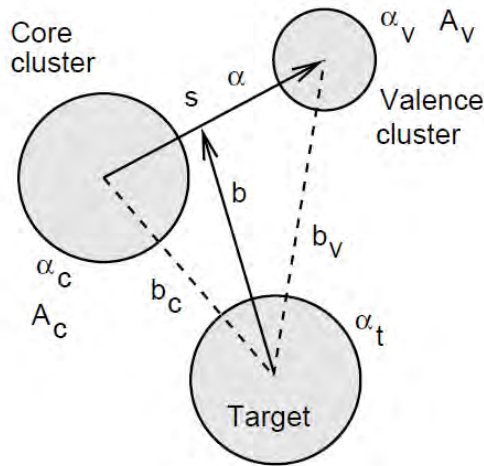


**Figure 1**-The two-cluster projectile and target coordinates.

The mean squared radius of the composite projectile  $\langle r^2 \rangle_p$  satisfies

$$A_p \langle r^2 \rangle_p = A_c \langle r^2 \rangle_c + A_v \langle r^2 \rangle_v + \frac{A_v A_c}{A_p} \langle r^2 \rangle = \frac{3}{2} (A_v \hat{\alpha}_v^2 + A_c \hat{\alpha}_c^2) \quad (20)$$

This approach provides a projectile density with distinct components due to the valence and core clusters. Such simple two component forms can be employed for calculating the density distributions of light exotic nuclei and also employed as input to optical limit calculations of reaction cross sections. However, a particular projectile single particle density, described by a given  $(A_c, A_v)$  mass split and choice of the two component ranges  $(\hat{\alpha}_c, \hat{\alpha}_v)$ , does not define the underlying structure of the projectile. If one of the original clusters is point like, for example  $\alpha_v = 0$ , then fixing  $\hat{\alpha}_v$  and  $\hat{\alpha}_c$  uniquely determines  $\alpha$  and hence  $\alpha_c$ .

The reaction cross sections for considered exotic nuclei are studied by Glauber model [29], where the internal motions of particles within the projectile ( $P$ ) and target ( $T$ ) are assumed slow compared to the relative motion of centers of mass of the projectile and target. The reaction cross section for a projectile incident upon a target is given by [30]

$$\sigma_R = 2\pi \int_0^\infty b [1 - T(b)] db \left( 1 - \frac{B_c}{E_{cm}} \right), \quad (21)$$

where  $B_c$  is Coulomb barrier,  $E_{cm}$  is the kinetic energy in the center of mass system and  $T(b)$  is the transparency function at impact parameter  $b$ . A straightforward calculation of  $T(b)$  is very complicated. One of the simplest methods to calculate  $T(b)$  is the Optical limit (OL) approximation. In this approximation, which ignores any correlations between particles in the projectile or target,  $T(b)$  is written as the squared modulus of the elastic  $S$ -matrix for the projectile-target system [31]

$$T(b) = |S_{el}^{OL}(b)|^2, \quad (22)$$

where

$$S_{el}^{OL}(b) = \exp[iO_{PT}(b)], \quad (23)$$

and

$$O_{PT}(b) = \int_{-\infty}^{\infty} dR_3 \int d\vec{r}_1 \int d\vec{r}_2 \rho_P(r_1) \rho_T(r_2) f_{NN}(\left| \vec{R} + \vec{r}_1 - \vec{r}_2 \right|) \quad (24)$$

is the overlap of the projectile and target ground state densities ( $\rho_P$  and  $\rho_T$ , respectively) with an effective nucleon-nucleon ( $NN$ ) amplitude [ $f_{NN}(r)$ ] integrated along the assumed straight line path of the projectile's center of mass at impact parameter  $b$ . For zero-range  $NN$  amplitude and isospin  $T = 0$  target,  $f_{NN}(r)$  has the form [31]

$$f_{NN}(r) = (i\bar{\sigma}_{NN}/2)\delta(r) \quad (25)$$

where  $\bar{\sigma}_{NN}$  is the average of the free neutron-neutron ( $nn$ ) and neutron-proton ( $np$ ) total cross section at the energy of interest. An explicit form for  $\bar{\sigma}_{NN}$  is given in ref. [32].

Expressing the projectile-target separation in cylindrical coordinates  $\vec{R} = (\vec{b}, R_3)$ , where  $z = 3$  is the axis chosen along the incident beam direction, then [with the help of Eqs. (24) and (25)] Eq. (23) gives

$$S_{el}^{OL}(b) = \exp \left[ -\frac{\bar{\sigma}_{NN}}{2} \int d\vec{r}_1 \int d\vec{r}_2 \rho_P^z(r_1) \rho_T^z(r_2) \delta(\left| \vec{b} + \vec{r}_1 - \vec{r}_2 \right|) \right]. \quad (26)$$

Integrating over the coordinates  $r_2$  then replacing  $r_1$  by  $s$ , we obtain

$$S_{el}^{OL}(b) = \exp \left[ -\frac{\bar{\sigma}_{NN}}{2} \int d\vec{s} \rho_P^z(s) \rho_T^z(\left| \vec{b} + \vec{s} \right|) \right], \quad (27)$$

where  $\rho_{P(T)}^z(s)$  is the  $z$ -direction integrated nucleon density distribution expressed as

$$\rho_{P(T)}^z(s) = \int_{-\infty}^{\infty} \rho_{P(T)}(\sqrt{s^2 + z^2}) dz. \quad (28)$$

It is obvious from Eq. (27) that the calculations of  $S_{el}^{OL}(b)$  requires only the projectile and target ground state densities. For simplicity, both densities are described by single Gaussian functions with range parameters  $\alpha_P$  and  $\alpha_T$ , respectively.

### Results and discussion

The ground state proton, neutron and matter densities of exotic one-proton halo nuclei  ${}^9\text{C}$  ( $S_p=1.30$  MeV,  $\tau_{1/2}=126.5$  ms) [33, 34],  ${}^{12}\text{N}$  ( $S_p=0.6$  MeV,  $\tau_{1/2}=11.0$  ms) [33, 34] and  ${}^{23}\text{Al}$  ( $S_p=0.122$  MeV,  $\tau_{1/2}=470$  ms) [33, 34] are studied by means of the TFSM [28] and BCM [29].

In TFSM, the calculations are based on using different model spaces for the core and valence (halo) protons. The single particle harmonic oscillator wave functions are employed with two different size parameters  $\beta_c$  and  $\beta_v$ . The nucleus  ${}^9\text{C}$  ( $J^\pi, T = 3/2^-, 3/2$ ) is formed by coupling the core  ${}^8\text{B}$  ( $J^\pi, T = 2^+, 1$ ) with the valence one proton ( $J^\pi, T = 1/2^-, 1/2$ ). The nucleus  ${}^{12}\text{N}$  ( $J^\pi, T = 1^+, 1$ ) is formed by coupling the core  ${}^{11}\text{C}$  ( $J^\pi, T = 3/2^-, 1/2$ ) with the valence one proton ( $J^\pi, T = 1/2^-, 1/2$ ). The nucleus  ${}^{23}\text{Al}$  ( $J^\pi, T = 1/2^+, 3/2$ ) is formed by coupling the core  ${}^{22}\text{Mg}$  ( $J^\pi, T = 0^+, 1$ ) with the valence one proton ( $J^\pi, T = 1/2^+, 1/2$ ). The valence (halo) proton in  ${}^9\text{C}$  and  ${}^{12}\text{N}$  is assumed to be in a pure  $1p_{1/2}$  while that in  ${}^{23}\text{Al}$  is considered as admixture between two configurations [ ${}^{22}\text{Mg}(0^+) \otimes v_{2s_{1/2}}$ ] $_{J=1/2^+}$  and [ ${}^{22}\text{Mg}(2^+) \otimes v_{1d_{5/2}}$ ] $_{J=1/2^+}$ , where  $v_{2s_{1/2}}$  and  $v_{1d_{5/2}}$  refer to the valence proton wave functions of  $2s_{1/2}$  and  $1d_{5/2}$  with occupation probabilities of 0.55 (in  $2s_{1/2}$ ) and 0.45 (in  $1d_{5/2}$ ) for the halo proton, respectively.

The matter density distribution of the halo nucleus  ${}^{23}\text{Al}$  is obtained by adding the density of the core to that of the valence (halo) proton. For simplicity, the density distributions of the ground ( $J^\pi, T = 0^+, 1$ ) and excited ( $J^\pi, T = 2^+, 1$ ) states of  ${}^{22}\text{Mg}$  are supposed to be the same as in Ref.

[16]. The configurations  $\{(1s_{1/2})^4, (1p_{3/2})^4\}$ ,  $\{(1s_{1/2})^4, (1p_{3/2})^7\}$  and  $\{(1s_{1/2})^4, (1p_{3/2})^8, (1p_{1/2})^4, (1d_{5/2})^6\}$  are assumed for core nuclei  ${}^8\text{B}$ ,  ${}^{11}\text{C}$  and  ${}^{22}\text{Mg}$ , respectively.

Table (1) displays the values of the harmonic oscillator size parameter  $\beta_c$  and  $\beta_v$  utilized in the present calculations for  ${}^9\text{C}$ ,  ${}^{12}\text{N}$  and  ${}^{23}\text{Al}$  exotic nuclei. It is clear from this table that the calculated rms matter radii for core [ ${}^8\text{B}$ ,  ${}^{11}\text{C}$  and  ${}^{22}\text{Mg}$ ] and exotic nuclei [ ${}^9\text{C}$ ,  ${}^{12}\text{N}$  and  ${}^{23}\text{Al}$ ], using these values of  $\beta_c$  and  $\beta_v$ , are in very good agreement with those of experimental results.

**Table 1**-Parameters for  $\beta_c$  and  $\beta_v$  utilized in the TFMSM of the present study together with the calculated and experimental rms radii of  ${}^9\text{C}$ ,  ${}^{12}\text{N}$  and  ${}^{23}\text{Al}$  exotic nuclei.

Exotic nuclei	Core nuclei	$\beta_c$ (fm)	$\beta_v$ (fm)	rms matter radii for core nuclei $\langle r^2 \rangle_{core}^{1/2}$ (fm)		rms matter radii for exotic nuclei $\langle r^2 \rangle_{exotic}^{1/2}$ (fm)	
				Calculated results	Experimental results	Calculated results	Experimental results
${}^9\text{C}$	${}^8\text{B}$	1.683	3.805	2.38	2.38±0.04 [35]	3.00	2.75±0.34 [36]
${}^{12}\text{N}$	${}^{11}\text{C}$	1.485	3.035	2.17	2.18±0.26 [36]	2.49	2.49±0.24 [36]
${}^{23}\text{Al}$	${}^{22}\text{Mg}$	1.728	3.785	2.78	2.78±0.26 [37]	3.09	2.905±0.25 [6]

In BCM [29], the halo nucleus is considered as a composite projectile consisting of core and valence clusters bounded in a state of relative motion figure.1. The internal densities of the clusters, given by Eq. (16), are described by single particle Gaussian wave functions. The composite projectile densities of  ${}^9\text{C}$ ,  ${}^{12}\text{N}$  and  ${}^{23}\text{Al}$  are calculated by Eq. (18).

Figure 2 shows the calculated matter density distributions (solid lines) obtained via TFMSM figures. 2(a), 2(c) and 2(e) and BCM figures. 2(b), 2(d) and 2(f)]. The top, middle and bottom panels correspond to halo nuclei  ${}^9\text{C}$ ,  ${}^{12}\text{N}$  and  ${}^{23}\text{Al}$ , respectively. The contributions of the core (dashed lines) and the halo proton (dash-dotted lines) to the matter densities are also shown in these figures. The experimental matter densities of  ${}^9\text{C}$  [12],  ${}^{12}\text{N}$  [38] (denoted by filled circle symbols) and  ${}^{23}\text{Al}$  [16] (denoted by the shaded area) are also displayed for comparison. The long tail behavior (which is a distinctive feature of halo nuclei) is revealed in all solid lines of figure 2. This behavior is in agreement with the experimental data mentioned above.

Figure 3 demonstrates the results as in figure. 2 but for the calculated neutron and proton density distributions displayed as dashed and dash-dotted lines, respectively. The long tail performance is clearly noticed in the dash-dotted lines. This performance is associated to the existence of the valence proton in the halo orbits. The steep slope performance is obviously observed in the dashed lines due to the absence of neutrons in the halo orbit, where all neutrons of these nuclei are found in its core only. The difference between the calculated proton and neutron rms radii is  $\Delta R = R_p - R_n = 3.31 - 2.27 = 1.04$  fm for  ${}^9\text{C}$ ,  $\Delta R = R_p - R_n = 2.71 - 2.15 = 0.56$  fm for  ${}^{12}\text{N}$  and  $\Delta R = R_p - R_n = 3.34 - 2.73 = 0.61$  fm for  ${}^{23}\text{Al}$ . This difference gives a supplementary support for the halo structure of these nuclei.

Figure 4 exhibits the comparison between the calculated matter density distribution of unstable nuclei  ${}^9\text{C}$ ,  ${}^{12}\text{N}$  and  ${}^{23}\text{Al}$  (solid lines) and those of stable nuclei  ${}^{12}\text{C}$ ,  ${}^{14}\text{N}$  and  ${}^{27}\text{Al}$  (dashed lines). To reproduce the experimental matter rms radii [ $2.481 \pm 0.08$ ,  $2.47 \pm 0.03$ ,  $3.03 \pm 0.02$ ] fm [35, 39] for the stable [ ${}^{12}\text{C}$ ,  ${}^{14}\text{N}$ ,  ${}^{27}\text{Al}$ ] nuclei, we utilize a value for the parameter [ $\beta = 1.686, 1.660, 1.825$ ] fm respectively. The calculated densities in figures. 4(a), 4(c) and 4(e) [obtained via TFMSM] are compared with corresponding densities in figures. 4(b), 4(d) and 4(f) [obtained via BCM]. It is clear from these figures that the solid and dashed lines are diverse. As the valence proton in [ ${}^9\text{C}$ ,  ${}^{12}\text{N}$ ,  ${}^{23}\text{Al}$ ] is weakly bound, the solid line has a longer tail than that of the dashed line. Figures 3 and 4 provide the conclusion that the halo phenomenon in  ${}^9\text{C}$ ,  ${}^{12}\text{N}$  and  ${}^{23}\text{Al}$  is connected to the valence proton but not to the core nucleons.

Elastic electron scattering proton form factors, which are simply given as Fourier transform of the ground state proton density distributions, for these halo nuclei are also calculated via the plane wave

born approximation (PWBA). As the calculations in the BCM do not distinguish between protons and neutrons, the calculations of the proton form factors are restricted only by the TFSM.

Figure 5 illustrates the comparison between the calculated elastic proton form factors of unstable (halo) nuclei (solid lines) and those of stable nuclei (dashed lines). The calculated proton form factors in figures. 5(a), 5(b) and 5(c) correspond to pairs of ( ${}^9\text{C}$ ,  ${}^{12}\text{C}$ ), ( ${}^{12}\text{N}$ ,  ${}^{14}\text{N}$ ) and ( ${}^{23}\text{Al}$ ,  ${}^{27}\text{Al}$ ) nuclei, respectively. The major difference between the calculated form factor of unstable [ ${}^9\text{C}$ ,  ${}^{12}\text{N}$ ,  ${}^{23}\text{Al}$ ] nuclei and those of stable [ ${}^{12}\text{C}$ ,  ${}^{14}\text{N}$ ,  ${}^{27}\text{Al}$ ] nuclei is attributed firstly to the influence of the proton density distributions of the last proton in unstable nuclei and secondly to the difference in the center of mass correction which depends on the mass number and the size parameter  $\beta$  (which is assumed in this case equal to the average of  $\beta_c$  and  $\beta_v$ ). It is clearly noticed in figures. 5(a) and (b), that each of the solid line and the dashed line has one diffraction minimum, while those in figure. 5(c) each has two diffraction minimum.

The reaction cross sections ( $\sigma_R$ ) are studied by means of the Glauber model with an optical limit approximation at high energies for  ${}^9\text{C}$ ,  ${}^{12}\text{N}$  and  ${}^{23}\text{Al}$  projectiles incident on the  ${}^{12}\text{C}$  target using the ground state densities of these nuclei. The densities of the projectile and target are described by single Gaussian functions with range parameters  $\alpha_p$  and  $\alpha_t$  for projectile and target nuclei, respectively. The calculated reaction cross sections are listed in table 2 along with the corresponding experimental data taken from [6, 35]. The calculated  $\sigma_R$  at 720 MeV for  ${}^9\text{C}+{}^{12}\text{C}$  system is 834 mb, which agrees well with the corresponding experimental data  $834 \pm 18$  mb [35]. The calculated  $\sigma_R$  at 720 MeV for  ${}^{12}\text{N}+{}^{12}\text{C}$  system is 856 mb, which agrees well with the corresponding experimental data  $856 \pm 55$  mb [35]. The calculated  $\sigma_R$  at 950 MeV for  ${}^{23}\text{Al}+{}^{12}\text{C}$  system is 1208 mb, which agrees well with the corresponding experimental data  $1208 \pm 68$  mb [6].

**Table 2-**Calculated reaction cross sections for  ${}^9\text{C}$ ,  ${}^{12}\text{N}$  and  ${}^{23}\text{Al}$  exotic nuclei.

Exotic Nuclei	Experimental rms radii (fm)	Calculated $\sigma_R$ (mb)	Experimental $\sigma_R$ (mb)	Energy (MeV)
${}^9\text{C}$	$2.75 \pm 0.34$ [36]	834	$834 \pm 18$ [35]	720
${}^{12}\text{N}$	$2.49 \pm 0.24$ [36]	856	$856 \pm 55$ [35]	720
${}^{23}\text{Al}$	$2.905 \pm 0.25$ [6]	1208	$1208 \pm 68$ [6]	950

### Summary and conclusions

The ground state proton, neutron and matter densities of exotic one-proton halo nuclei  ${}^9\text{C}$ ,  ${}^{12}\text{N}$  and  ${}^{23}\text{Al}$  are studied by means of the TFSM and BCM. The long tail performance, presumed as a typical property for the halo structure, is clearly revealed in the calculated proton and matter density distributions of these exotic nuclei. Moreover, the noticeable difference which is found between the calculated overall proton and neutron rms radii as well provides a supplementary support for the halo structure of these nuclei.

Elastic electron scattering proton form factors for these exotic halo nuclei are also studied using the TFSM. It is found that the major difference between the calculated form factors of unstable [ ${}^9\text{C}$ ,  ${}^{12}\text{N}$ ,  ${}^{23}\text{Al}$ ] nuclei and those of stable [ ${}^{12}\text{C}$ ,  ${}^{14}\text{N}$ ,  ${}^{27}\text{Al}$ ] nuclei is attributed firstly to the influence of the proton density distributions of the last proton in unstable nuclei and secondly to the difference in the center of mass correction which depends on the mass number and the size parameter  $\beta$  (which is assumed in this case equal to the average of  $\beta_c$  and  $\beta_v$ ).

The reaction cross sections for these exotic nuclei are studied by means of the Glauber model with an optical limit approximation using the ground state densities of the projectile and target, where these densities are described by single Gaussian functions. The calculated reaction cross sections at high energy are in agreement with the measured data.

The analysis of the present study suggests that the structure of the valence proton in  ${}^9\text{C}$  and  ${}^{12}\text{N}$  is a pure ( $1p_{1/2}$ ) configuration while that for  ${}^{23}\text{Al}$  is mixed configurations with dominant ( $2s_{1/2}$ ). The present study supports the halo structure of these nuclei.

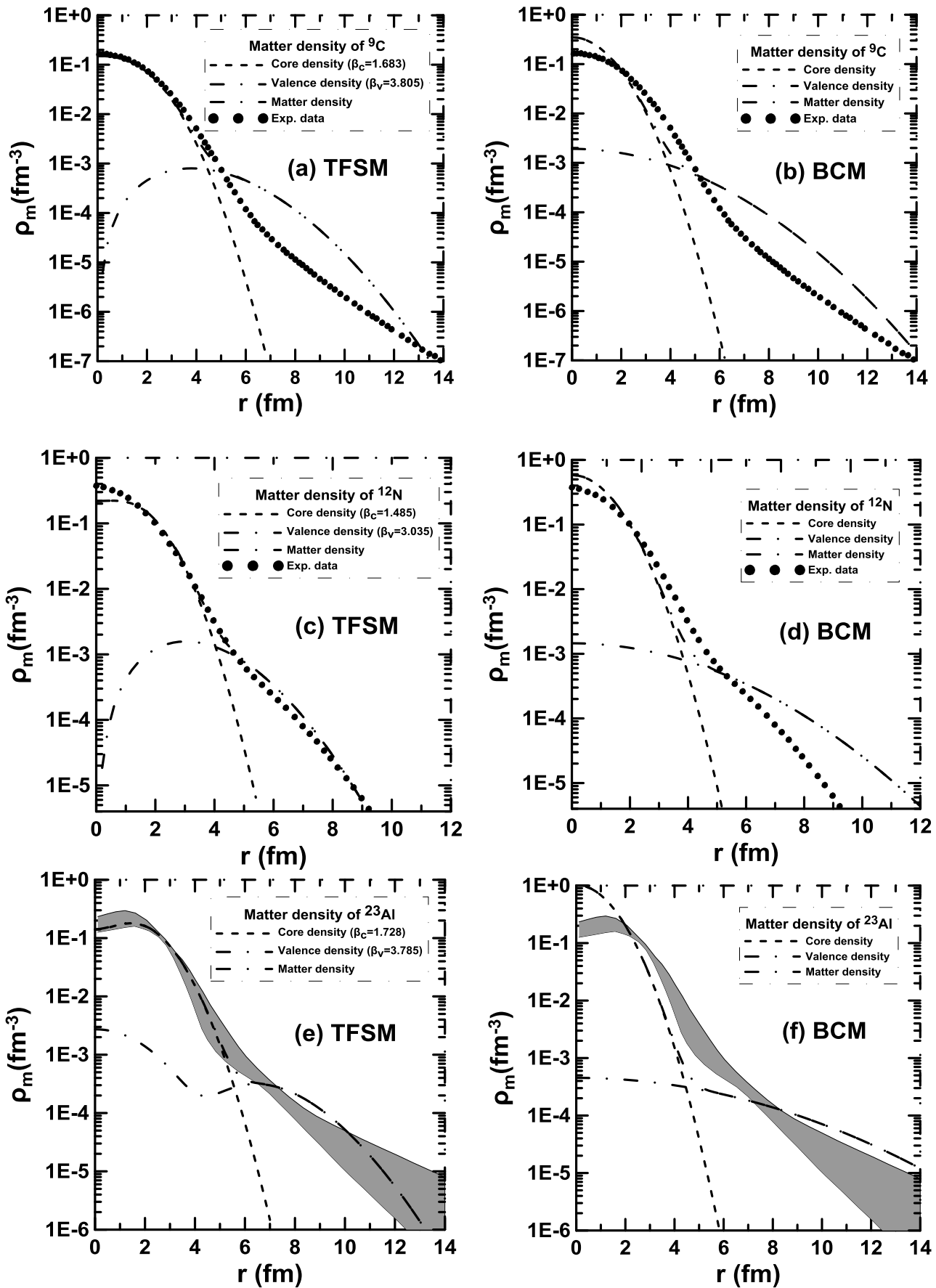


Figure 2-The calculated matter density distributions obtained via TFMSM and BCM.

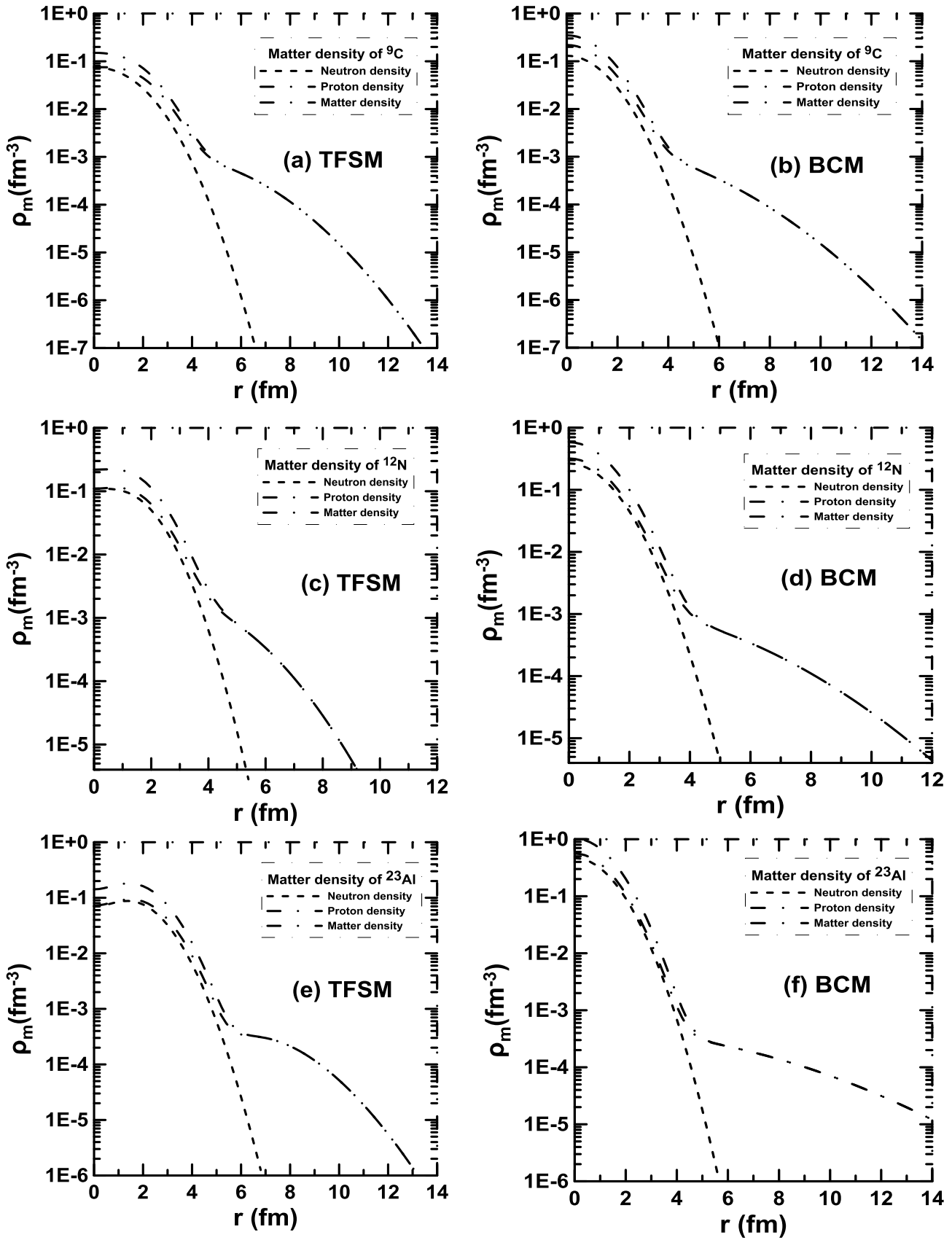


Figure 3-Neutron, proton and matter density distributions obtained via TFMS and BCM.

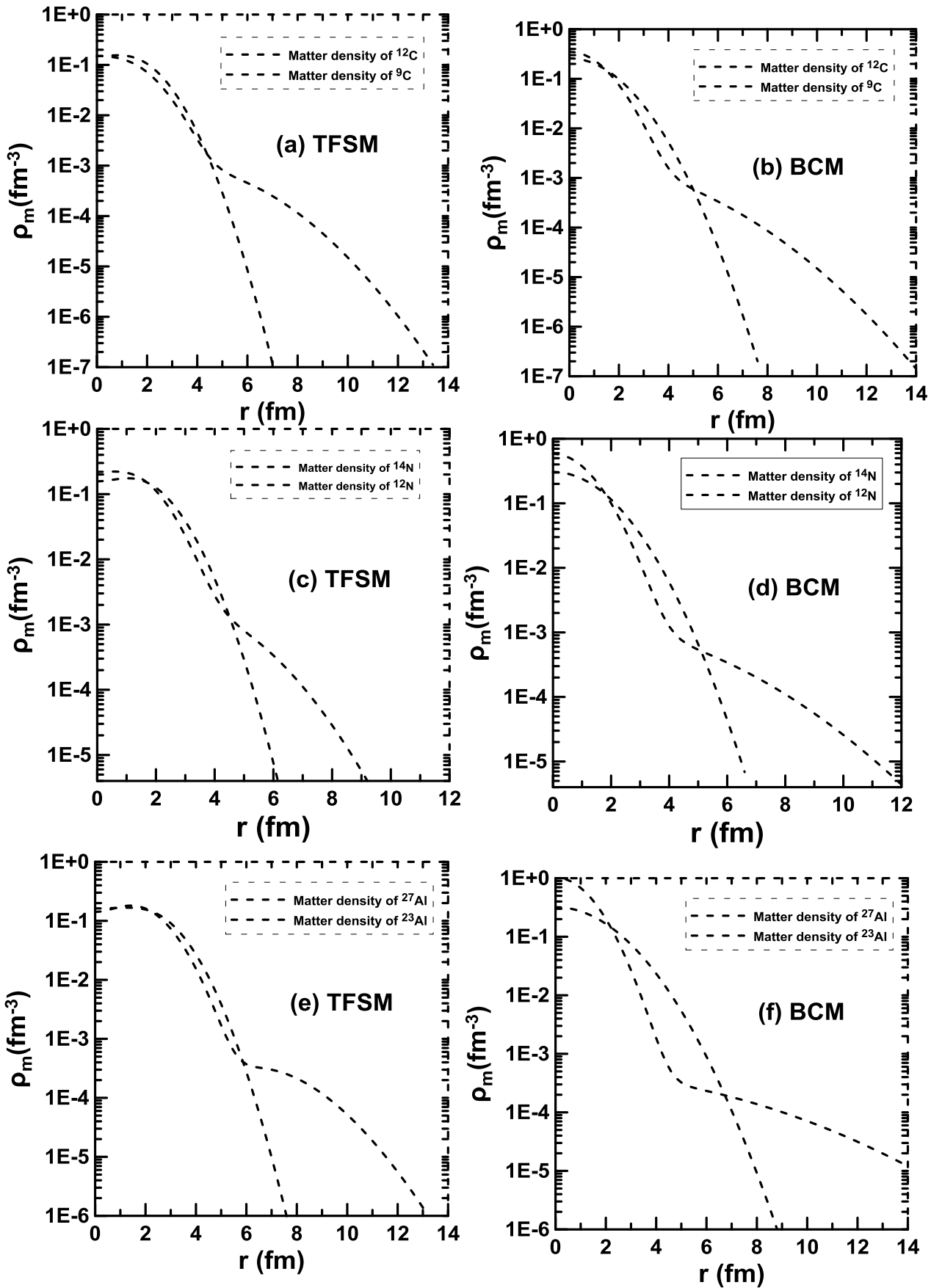
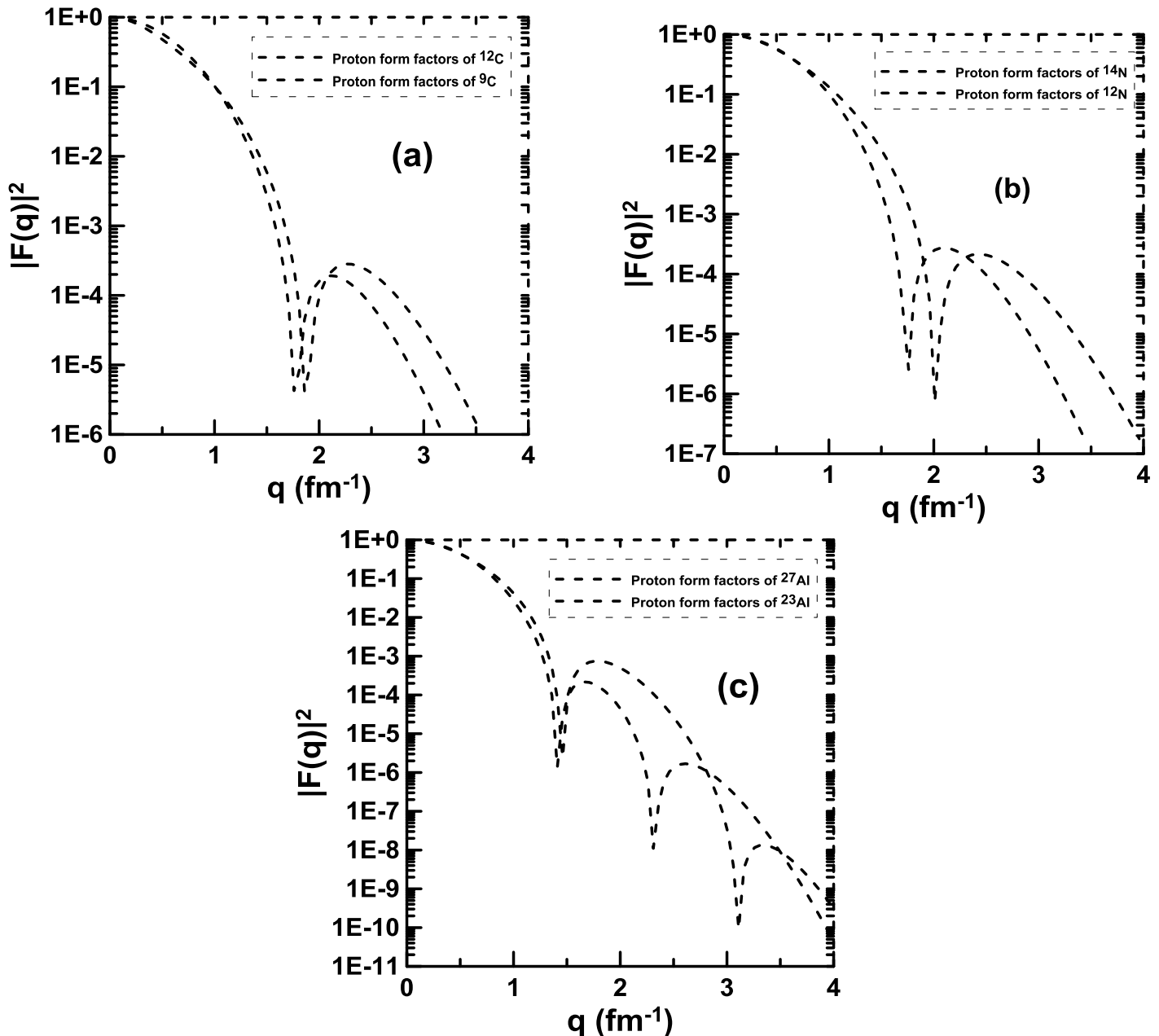


Figure 4-The comparison between the calculated matter density of unstable and stable nuclei.



**Figure 5-**The comparison between the calculated proton form factors of unstable (exotic) nuclei and those of stable nuclei.

### References

- 1- Tanihata I., Hamagaki H., Hashimoto O., Shida Y., Yoshikawa N., Sugimoto K., Yamakawa O, and Kobayashi T. **1985**. Measurement of interaction cross sections and nuclear radii in the light p-shell region. *Physical Review Letters*, **55** (24), pp: 2676-2679.
- 2- Hansen P. G. and Jonson B. **1987**. The neutron halo of extremely neutron-rich nuclei. *Europhysics Letters*, **4**(4), pp: 409-414.
- 3- Nakamura T., Kobayashi N., Kondo Y., Satou Y., Aoi N., Baba H., Deguchi S., Fukuda N., Gibelin J., Inabe N., Ishihara M., Kameda D., Kawada Y., Kubo T., Kusaka K., Mengoni A., Motobayashi T., Ohnishi T., Ohtake M., Orr N. A., Otsu H., Otsuka T., Saito A., Sakurai H., Shimoura S., Sumikama T., Takeda H., Takeshita E., Takechi M., Takeuchi S., Tanaka K., Tanaka K. N., Tanaka N., Togano Y., Utsuno Y., Yoneda K., Yoshida A., and Yoshida K. **2009**. Halo Structure of the Island of Inversion Nucleus  $^{31}\text{Ne}$ . *Physical Review Letters* 103 (262501), pp: 1-4.

- 4- Wang Z. and Ren Z. Z. **2004**. Probing proton halo of the exotic nucleus  $^{28}\text{S}$  by elastic electron scattering. *Science in China Series G Physics and Astronomy* 47, pp: 42-51.
- 5- Blank B., Marchand C., Pravikoff M.S., Baumann T., Bou F., Geissel H., Hellström M., Iwasa N., Schwab W., Sammerer K. and Gai M. **1997**. Total interaction and proton-removal cross-section measurements for the proton-rich isotopes  $^7\text{Be}$ ,  $^8\text{B}$ , and  $^9\text{C}$  *Nuclear Physics A* 624, pp: 242-256.
- 6- Zhang H.Y., Shen W.Q., Ren Z.Z., Ma Y.G., Jiang W.Z., Zhu Z.Y., Cai X.Z., Fang D.Q., Zhong C., Yu L.P., Wei Y.B., Zhan W.L., Guo Z.Y., Xiao G.Q., Wang J.S., Wang J.C., Wang Q.J., Li J.X., Wang M. and Chen Z.Q. **2002**. Measurement of reaction cross section for proton-rich nuclei ( $A < 30$ ) at intermediate energies. *Nuclear Physics A* 707, pp: 303–324.
- 7- Anis D. **2012**. Nuclear processes in intense light matter interaction. Ph.D. Thesis, Department of physics, College of Science, University of Heidelberg, Germany.
- 8- Wang Z. and Ren Z. Z. **2004**. Elastic electron scattering on exotic light proton-rich nuclei. *Physical Review C* 70, (034303), pp: 1-9.
- 9- Haik Simon, **2005**. Technical Proposal for the Design, Construction, commissioning, and operation of the ELISe setup, GSI *Internal Report*.
- 10- Suda T. and Wakasugi M. **2005**. Structure studies of unstable nuclei by electron scattering. *Progress in Particle and Nuclear Physics*. 55, pp: 417-436.
- 11- Ozawa A., Tanihata I., Kobayashi T., Sugahara Y., Yamakawa O., Omata K., Sugimoto K., Olson D., Christie W. and Wieman H. **1996**. Interaction cross sections and radii of light nuclei. *Nuclear Physics A* 608, pp: 63-76.
- 12- Hong L. Z., Bing G., Ping L. W., Xiang B. X., Gang L., Jun S., Quan Y. S., Xiang W. B., Sheng Z. **2005**. Radius of  $^9\text{C}$  from the Asymptotic Normalization Coefficient. *Chinese Physics Letter* 22, pp: 1870-1872.
- 13- Ozawa A., Tanihata I., Kobayashi T., Hirata D., Yamakawa O., Omata K., Takahashi N., Shimoda T., Sugimoto K., Olson D., Christie W. and Wieman H. **1995**. Interaction cross sections and radii of  $^{11}\text{C}$  and  $^{12}\text{N}$  and effective deformation parameters in light mirror nuclei. *Nuclear Physics A* 583, pp: 807-810.
- 14- Warner R. E., Thirumurthy H., Woodroffe J., Becchetti F. D., Brown J. A., Davids B. S., Galonsky A., Kolata J. J., Kruse J. J., Lee M. Y., Nadasen A., O'Donnell T. W., Roberts D. A., Ronningen R. M., Samanta, C., Schwandt P., Schwarzenberg J., Steiner M., Subotic K., Wang J. and Simmerman J. A. **1998**. Reaction cross sections in Si of light proton-halo candidates  $^{12}\text{N}$  and  $^{17}\text{Ne}$ . *Nuclear Physics A* 635, pp: 292-304.
- 15- Zhang H. Y., Shen W. Q., Ren Z. Z., Ma Y. G., Cai X. Z., Zhong C., Wei Y. B. and Chen J. G. **2002**. Possible  $1d_{5/2}$  and  $2s_{1/2}$  level inversion in the proton rich nucleus  $^{23}\text{Al}$ . *Chinese Physics Letter* 19, pp: 1599-1601.
- 16- Fang D. Q., Ma C. W., Ma Y. G., Cai X. Z., Chen J. G., Shen J. H., Guo W., Tian W. D., Wang K., Wei Y. B., Yan T. Z., Zhong C., Zuo J. X. and Shen W. Q. **2005**. One proton halo structure in  $^{23}\text{Al}$ . *Chinese Physics Letter* 22, pp: 572-575.
- 17- Cai X., Feng J., Shen W., Ma Y., Wang J. and Ye W. **1998**. In-medium nucleon-nucleon cross section and its effect on total nuclear reaction cross section. *Physical Review C* 58, pp 572-575.
- 18- Tanihata I., Hirata D., Kobayashi T., Shirnoura S., Sugimoto K. and Toki H. **1992**. Revelation of thick neutron skins in nuclei. *Physics Letters. B* 289, pp: 261-266.
- 19- Tetsuaki M. **2011**. Density distributions for two neutron halo nuclei  $^{11}\text{Li}$  and  $^{14}\text{Be}$  deduced by the reaction cross section measurements. Ph.D. Thesis. Department of physics, College of Science, University of Tsukuba.
- 20- Ogawa Y., Yabanab K. and Suzuki Y. **1992**. Glauber model analysis of the fragmentation reaction cross sections of  $^{11}\text{Li}$ . *Nuclear Physics A* 543, pp: 722-750.
- 21- Ozawa A., Baumann T., Chulkov L., Cortina D., Datta U., Fernandez J., Geissel H., Hammache F., Itahashi K., Ivanov M., Janik R., Kato T., Kimura K., Kobayashi T., Markenroth K., Meister M., Münzenberg G., Ohtsubo T., Ohya S., Okuda T., Ogloblin A.A., Pribora V., Sekiguchi M., Sitár B., Strmen P., Sugimoto S., Sümmerer K., Suzuki T., Tanihata I. and Yamaguchi Y. **2002**. Measurements of the interaction cross sections for Ar and Cl isotopes. *Nuclear Physics A* 709, pp: 60–72.

- 22- Guo W. J., Jiang H. Q., Liu J. Y., Zuo W., Ren Z. Z., and Lee X. G. **2003**. Total nuclear reaction cross section induced by halo nuclei and stable nuclei. *Commun. Theoretical Physics*. (Beijing, China) 40 , pp: 577–584.
- 23- Tanihata I. **1996**. Neutron halo nuclei. *J. Phys. G* **22**, pp: 157-198.
- 24- Zhao Y.L., Ma Z.Y., Chen B.Q. and Sun X.Q. **2001**. Extended Glauber theory and its application in halo nucleus scattering. *High Energy Phys. Nuclear Physics* **6**,pp. 506.
- 25- Brown B. A., Radhi R. and Wildenthal B. H. **1983**. Electric quadrupole and hexadecupole nuclear excitations from the perspectives of electron scattering and modern shell-model theory. *Physics Reports*. **101**(5),pp: 313-358.
- 26- Brown B. A., Etchegoyen A., Godwin N. S., Rae W. D. M., Richter W. A., Ormand W.E., Warburton E. K., Winfield J. S., Zhao L., Zimmerman C. H. **2005**. Oxbash for Windows PC. MSU-NSCL report number 1289.
- 27- Kuo T. T. S., Muether H. and Amir-Azimi-Nili K. **1996**. Realistic effective interactions for halo nuclei. *Nuclear Physics A*. **606**, pp: 15-26.
- 28- Kuo T. T. S., Krmpotic F. and Tzeng Y. **1997**. Suppression of core polarization in halo nuclei. *Physical Review Letter* **78**(14), pp: 2708-2711.
- 29- Tostevin J. A., Johnson R. C. and Al-Khalili J. S. **1998**. Manifestation of halo size in scattering and reactions. *Nuclear Physics A* **630**, pp: 340c-351c.
- 30- Zheng T., Yamaguchi T., Ozawa A., Chiba M., Kanungo R., Kato T., Katori K., Morimoto K., Ohnishi T., Suda T., Tanihata I., Yamaguchi Y., Yoshida A., Yoshida K., Toki H. and Nakajima N. **2002**. Study of halo structure of  $^{16}\text{C}$  from reaction cross section measurement. *Nuclear Physics A* **709**, pp: 103-118.
- 31- Tostevin J. A. and Al-Khalili J. S. **1997**. How large are the halos of light nuclei. *Nuclear Physics A* **616** , pp: 418c-425c.
- 32- Charagi S.K. and Gupta S.K. **1990**. Coulomb-modified Glauber model description of heavy-ion reaction cross sections. *Physical Review C* **41**, pp: 1610-1618.
- 33- Audi G, Wapstra A H and Thibault C. **2003**. The AME 2003 atomic mass evaluation (II). Tables, graphs and references. *Nuclear Physics A* **729**, pp: 337–676.
- 34- Audi G., Bersillon O., Blachot J. and Wapstra A.H. **2003**. The NUBASE evaluation of nuclear and decay properties. *Nuclear Physics A* **729**, pp: 3-128.
- 35- Ozawa A., Suzuki T. and Tanihata I. **2001**. Nuclear size and related topics. *Nuclear Physics A* **693**,pp: 32–62.
- 36- Warner R. E., Carstoiu F., Brown J. A., Becchetti F. D. , Roberts D. A., Davids B., Galonsky A., Ronningen R. M., Steiner M., Horoi M., Kolata J. J., Nadasen A., Samanta C., Schwartzberg J. and Subotic K. **2006**. Reaction and proton-removal cross sections of  $^6\text{Li}$ ,  $^7\text{Be}$ ,  $^{10}\text{B}$ ,  $^{9,10,11}\text{C}$ ,  $^{12}\text{N}$ ,  $^{13,15}\text{O}$ , and  $^{17}\text{Ne}$  on Si at 15 to 53 MeV/nucleon. *Physical Review C* **74**, 014605, pp: 1-12.
- 37- Zhao Y. L., Ma Z. Y., Chen B. Q., and Shen W. Q. **2003**. Halo structure of nucleus  $^{23}\text{Al}$ . *Chinese Physics Letter* **20** (1), pp:53-55.
- 38- Xing L. J., Ping L. P., Song W. J., Guo H. Z., Shi M. R., Yu S. Z., Chen L., Fu C. R., Shan X. H., Qing X. G. and Yan G. Z. **2010**. Measurement of the total reaction cross section for the mirror nuclei  $^{12}\text{N}$  and  $^{12}\text{B}$ . *Chinese Physics C* **34**, pp: 452-455.
- 39- Vries H. D., De Jager C. W. and Vries C. D. **1987**. Nuclear charge density distribution parameters from elastic electron scattering. *Atomic Data and Nuclear Data Tables* **36**, pp: 495-536.